Biomass-Based Honeycomb-Like Architectures for Preparation of Robust Carbon Foams with High Electromagnetic Interference Shielding Performance

Zhihui Zeng[1], *Youfang Zhang*[1], *Xiu Yun Daphne Ma*[1], *Seyed Ismail Seyed Shahabadi*[1], *Boyang Che*[1], Peiyu Wang[2], *Xuehong Lu*[1,*]

[1]*School of Materials Science and Engineering, Nanyang Technological University, 50 Nanyang Avenue, Singapore 639798, Singapore*

[2]*State Key Laboratory for Turbulence and Complex Systems, College of Engineering, Peking University, Beijing 100871, China*

ABSTRACT: Honeycomb-like lignin-derived carbon (LC) foams doped with reduced graphene oxide (RGO) are fabricated via unidirectional ice-templating followed by freeze-drying and carbonization. The dimensions, constituent contents, and density of the foams could be easily adjusted. By manipulating the density, high electrical conductivity and good mechanical properties could be achieved at relatively low RGO contents. In addition to the high conductivity and interfaces between LC and RGO, aligned pores also boost electromagnetic interference (EMI) shielding effectiveness (SE) of the foams owing to induced multiple reflections. X-band EMI SE of the LC-based foams with 2-mm thickness could reach 28.5 to 70.5 dB at very low densities. Furthermore, the normalized surface specific SE (SE divided by density and thickness) could be as high as 28750 dB·cm^2/g, which is much higher than those of other types of carbon foams and most shielding materials ever reported. With the outstanding EMI shielding performance, good mechanical properties and more sustainable raw material, the biomass-based carbon foams offer promising prospects for lightweight, robust and high-performance EMI shielding materials.

* Corresponding author. E-mail address: asxhlu@ntu.edu.sg (Xuehong Lu).

1. Introduction

In recent years, electromagnetic pollution from rapidly growing number of electronic devices has caused increased electromagnetic interference (EMI), which disturbs the normal work of electronics and imposes adverse impacts on human health [1-4]. High-performance EMI shielding materials that can mitigate the transmission of electromagnetic waves efficiently are hence required for many applications. For example, lightweight, robust and high-performance EMI shielding materials are required for apparatus such as aircraft, spacecraft, and portable electronics [5-10]. The most commonly used shielding materials are metal-based shields, which however suffer from high density, propensity to corrosion and limited tunability of EMI shielding effectiveness (SE) [11-15]. On this account, carbon-based materials featuring excellent mechanical properties, low density, good chemical resistance and tunable SE are increasingly researched as promising high-performance EMI shielding materials [16-24]. In particular, micron-sized pores can be easily introduced into the carbon-based materials, drastically reducing the weight and introducing numerous interfaces between the voids and cell walls [4, 25-28]. The interfaces can enhance the multiple reflection of incident electromagnetic waves [8, 10, 14], which, combined with the intrinsic wave loss ability derived from the charge carriers in the carbon phase, renders the lightweight carbon-based porous architectures high EMI shielding performance. For example, the commercial carbon foam [29] is reported with an EMI SE of 40 dB at the thickness of 2 mm and a density of around 0.17 g/cm^3. Specific SE (SSE) [10, 13, 15], which is defined as SE of an EMI shielding material divided by its

density for describing both the lightweight and EMI shielding performance, can thus reach as large as 241 dB·cm^3/g for the aforementioned carbon foam, in comparison to 33.1 dB·cm^3/g for a 3.1 mm thick copper shield [11]. The CNT sponge prepared by chemical vapor deposition method also shows an SE of 22 dB and an SSE of 1100 dB·cm^3/g at a thickness of 2.38 mm [30].

The carbon-based porous architectures mainly include carbon foams [29-34], carbon fiber mats [35], CNT sponges [21, 36], and graphene-based porous architectures [24-28]. In contrast to the porous architectures constructed dominantly from carbon nanomaterials, such as CNTs and graphene sheets, amorphous carbon foams can be prepared easily by carbonization of low-cost materials such as polymer sponges [29, 34]. The polymer-derived carbon porous architectures can also be loaded with other additives such as metal or magnetic particles. Combined with the considerable electrical conductivity of the additives and charge carrier amount derived from the carbon constituent, such doped carbon foams show a high potential for EMI shielding applications. For example, polymer-derived carbon foams loaded with ferrocene [37] and MWCNT [30] showed EMI SE of 85 and 81 dB, and SSE of 130.0 and 163.5 dB·cm^3/g, respectively, at thickness of 2.75 mm. The reported polymer-derived carbon foams, including those loaded with additives, however, still showed relatively high densities because the low mechanical strength of their cell walls resulted in shrinkage or even collapse of the carbon foams at low densities. Meanwhile, the porosity, pore structure, and constituent of raw polymer sponges are not easy to adjust due to the restriction of traditional foaming method [22, 34, 38, 39],

limiting tunability of EMI shielding performance of the carbon foams. Moreover, it is also desirable to replace synthetic polymers with biomass-based raw materials to make EMI shielding materials more environmentally benign.

Lignin is one of the most abundant biomass materials [40-42] and accounts for up to 35 wt% of wood. This readily available and renewable biomass-based raw material can be obtained as a low-cost byproduct from paper industry and has a high carbon yield, which is beneficial to large-scale production of carbon foams. Our previous studies [43] showed that the presence of a small fraction of lignin-derived carbon (LC) in reduced graphene oxide (RGO)-based aerogels enhanced the interfacial polarization effect with little reduction in the amount of charge carriers and conductivity of graphene cell walls, as well as improved integrity of the cell walls for boosting multiple reflections. These render the ultralight RGO-based porous architectures improved EMI shielding performance compared with that of neat RGO aerogels. However, the major building block of the aerogels, graphene oxide (GO), could only be stably dispersed in water in a relatively narrow concentration range, limiting density of the resultant RGO-based aerogels, and hence constrain their mechanical strength and conductivity. Additionally, their EMI SE (up to 49 dB at 2 mm thickness) was not sufficiently high for some demanding applications. In the present work, our goal was to use predominantly lignin as the raw material to achieve robust and environmentally benign EMI shielding materials with high SE and SSE. We found that different from GO, lignin could form stable suspensions in a much wider range of concentrations, allowing the preparation of honeycomb-like lignin

foams with a remarkably wide range of densities via unidirectional freeze-drying method [44-46], whereas similar to polymer sponges, the subsequent carbonization would cause huge volume shrinkage of the foams. However, by simply dispersing a small amount of GO in lignin suspensions, the resultant carbon foams could exhibit greatly reduced volume shrinkage in carbonization owing to the excellent reinforcing effect of the uniformly distributed RGO in LC. This enables the facile manipulation of density and microstructure of the LC-based foams, also paving the way for tackling the electrical conductivity issue. The high content of LC in the foams will also give better integrated cell walls [43] and anisotropic micron-sized pores, providing more cell wall-void interfaces in the transverse direction (normal to the aligned cell walls direction). This could enhance the multiple reflection ability of the carbon foams, improving their EMI shielding performance. The interfaces between RGO and LC can also facilitate the creation of substantial interfacial dipoles in electromagnetic field, enhancing the polarization loss ability to the electromagnetic waves. Herein we demonstrate that EMI SE of the RGO-doped LC foams can reach more than 80.0 dB at a thickness of 2 mm. Moreover, the normalized surface specific SE (SSE/*d*, defined as SE divided by the density and thickness) can reach up to 28750 $dB \cdot cm^2/g$, which is much higher than that of other polymer-derived carbon foams as well as most shielding materials reported so far. This shows the great promise of the biomass-derived carbon architectures as high-performance EMI shielding materials.

2. Experimental

2.1. Materials and Preparation

2.1.1. Preparation of honeycomb-liked LC foams. The lignin aqueous solution with various concentrations was prepared via dispersing the alkali lignin (USA, TCI product number: L0082, soft lignin) into the water by magnetic mixing. The suspension was further cast in a Teflon container with a metal base that is immersed in the liquid nitrogen for freezing process. In the freezing process, the temperature gradient between the top and bottom side of the suspension in the mould led to the formation of ice crystals in the bottom side and the unidirectional growth towards the top side. In a subsequent of freeze-drying the frozen samples in a freeze-drying vessel (–80 ^{o}C and 10 Pa) for around 24 h, a type of honeycomb-like polymer foams with aligned micron-sized pores and cell walls were obtained. Subsequently, the polymer foams were heated at a rate of 5 ºC/min in a tube furnace and annealed at the temperature of 900 ºC for 2 h under argon atmosphere, leading to the fabrication of the honeycomb-like LC foams.

2.1.2. Preparation of honeycomb-like RGO-doped LC foams. In order to incorporate RGO into the LC foams, a GO aqueous suspension was prepared using a previous reported method [43, 47] and mixed with lignin solutions before the freezing process. The GO and lignin could interact with each other well because of their amphiphilic nature and the possibility of π-π interaction between aromatic rings of lignin and GO [40, 43]. After the same freeze-drying process and thermal annealing treatment, honeycomb-like RGO-doped carbon foams doped with reduced graphene oxide (RGO) [47] were obtained. Density of the foams could be controlled in a wide range from

several microgram to several hundred microgram per cubic centimeter by adjusting the water fraction of the aqueous suspension. Notably, although GO and annealed RGO foams could also be prepared using this method, the GO concentration in water was limited by the stability of the suspensions, resulting in relatively low densities (< 7 mg/cm^3) of the resultant RGO foams, and similar phenomenon was also reported by other researchers [48, 49]. Also, various shapes or sizes of the honeycomb-like RGO-doped LC foams could be achieved by selecting various molds, which was beneficial to satisfy diverse application occasions.

2.2. Characterization.

The microstructure of the porous architectures was investigated by scanning electron microscopy (SEM, JSM-7600F). X-ray diffraction (XRD) tests were carried out at room temperature using a specular reflection mode (Cu Ka radiation, PANalytical, Holland). A thermogravimetric analyzer (TGA, TA Instrument Q500) was employed to study the mass change in the carbonization process. The experiment was carried out from room temperature to 900°C in nitrogen atmosphere at a speed of 5 ℃/min. The resistance of the sample was measured by four-probe method using a Keithley 4200-SCS semiconductor characterization system (Keithley, Cleveland, Ohio, USA) to calculate the electrical conductivity. The measured electrical conductivities of the honeycomb-liked carbon-based foams were similar in different directions due to the interconnected cell walls. The compression behavior of the foams was evaluated by a dynamic mechanical analyzer (DMA, TA Q800), and at least five samples were tested for each component foam. EMI SE measurements were carried out on the samples

with dimensions of 22.86 mm × 10.16 mm × 2.0 mm in the frequency range of 8.2–12.4 GHz (X-band) by a waveguide method using a vector network analyzer (Agilent E8363B PNA-L), and more than five samples were tested for each component foam, the detailed test information can be described as shown in our previous work [13, 50].

3. Results and Discussion

3.1. Fabrication and properties of the honeycomb-like LC foams

The fabricated process of the honeycomb-like LC foams and the underlying mechanism is illustrated in Fig. 1. By unidirectionally freeze-drying the lignin aqueous suspension (Figure 1 a-b), honeycomb-like lignin foams composed of lignin cell walls and unidirectional pores in the longitudinal direction (parallel to the ice growth direction as shown in the arrow direction) are formed (Fig. 1c,d). These honeycomb-like free-standing foams are well sustained by the interconnected cell walls with considerable mechanical strength. Subsequently, the carbonization of lignin cell walls to amorphous carbon leads to LC foams, which can keep the honeycomb-like microstructure of the lignin foam (Fig. 1e, f). The XRD pattern of the lignin shows a relatively sharp peak at 22.5°, whereas the resultant LC only shows a broad carbon peak at around 24.5° (Fig. 1g). Since lignin is an aromatic macromolecular compound with three-dimensional links among methoxylated aromatic units [51, 52], TGA curves of lignin may reveal three regions. As shown in Fig. 1h, the initial weight loss step of lignin occurs at 30–120 °C, which originates from the evaporation of water absorbed. The weight loss during the second pyrolysis

step at around 300 °C is mainly ascribed to the cleaving of alkyl and methoxy groups, releasing methanol and phenolic compounds with hydroxyl group and alkyl groups. Finally, the third pyrolysis stage above 600 °C is ascribed to the decarbonylation reaction of alkyl side chains with carbonyl groups (-CHO), and also during this stage, functional groups are reduced to a large extent, facilitating the process of the formation of amorphous carbon. [53-55] Therefore, a large mass reduction of lignin in the carbonization process can lead to a large volume shrinkage of the foam as shown in Fig. 1i.

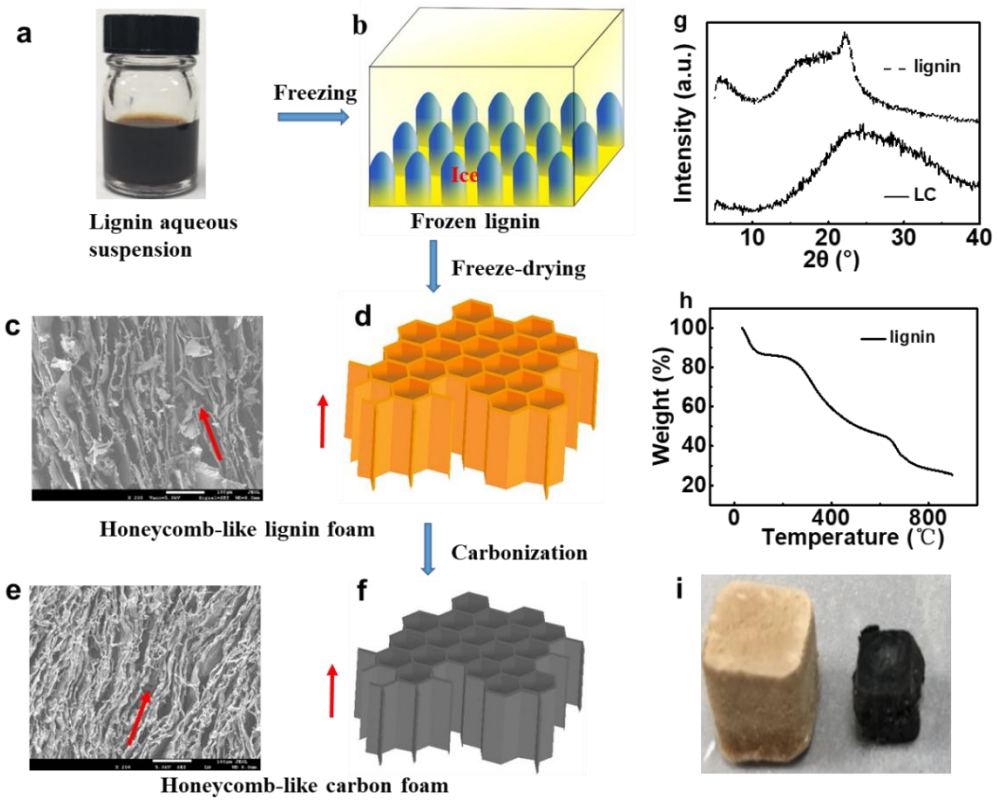

Fig. 1. The preparation process for the honeycomb-like LC foams: (a) images of lignin suspension; (b) unidirectional freezing mechanism; (c) microstructure of the lignin foam in the longitudinal direction (the arrow direction); (d) a schematic showing the as-prepared lignin foam; (e) microstructure of the LC foam in the longitudinal direction (the arrow direction), (f) a schematic showing the as-prepared LC foam; (g) XRD patterns of the lignin and LC; (h) TGA curve of the lignin; (i) optical images of the lignin foam (left) and resultant LC foams (right).

In the lignin suspension, the lignin concentration can be adjusted easily, rendering the as-prepared lignin foams and the resultant LC foams different microstructures. The average gap of tens of micrometers between the adjacent cell walls changes little for the lignin foams derived from the suspensions of different lignin concentrations as shown in Fig. 2a-b. However, a higher lignin concentration in the initial suspension leads to thicker cell walls of the foams. In the assembly process of honeycomb-like lignin foams, rapid formation of ice-crystal nuclei at the bottom of the suspension and the unidirectional growth of ice crystals take place. The lignin is excluded from the space occupied by the ice crystals to form the cell walls of submicron-sized thickness. Therefore, higher lignin concentration in the suspension can result in a thicker cell-wall thickness due to the nearly unchanged amount of crystal nuclei at a same frozen temperature, while the average gap between the cell walls is mainly determined by the final size of the crystals, for which no obvious change is observed in the SEM images, implying that lignin concentration does not affect crystal growth rate significantly in the studied lignin concentration range. This phenomenon is similar to that of polymer-based foams and has been clearly described in literatures [13, 15]. In the carbonization process, the macroscopic shrinkage correlates to a smaller average gap between adjacent cell walls for the LC foams (Fig. 2c, d). In addition, large cell walls with good integrity are observed for both the lignin and LC foams, which may be instrumental in the multiple reflection of incident waves for EMI shielding.

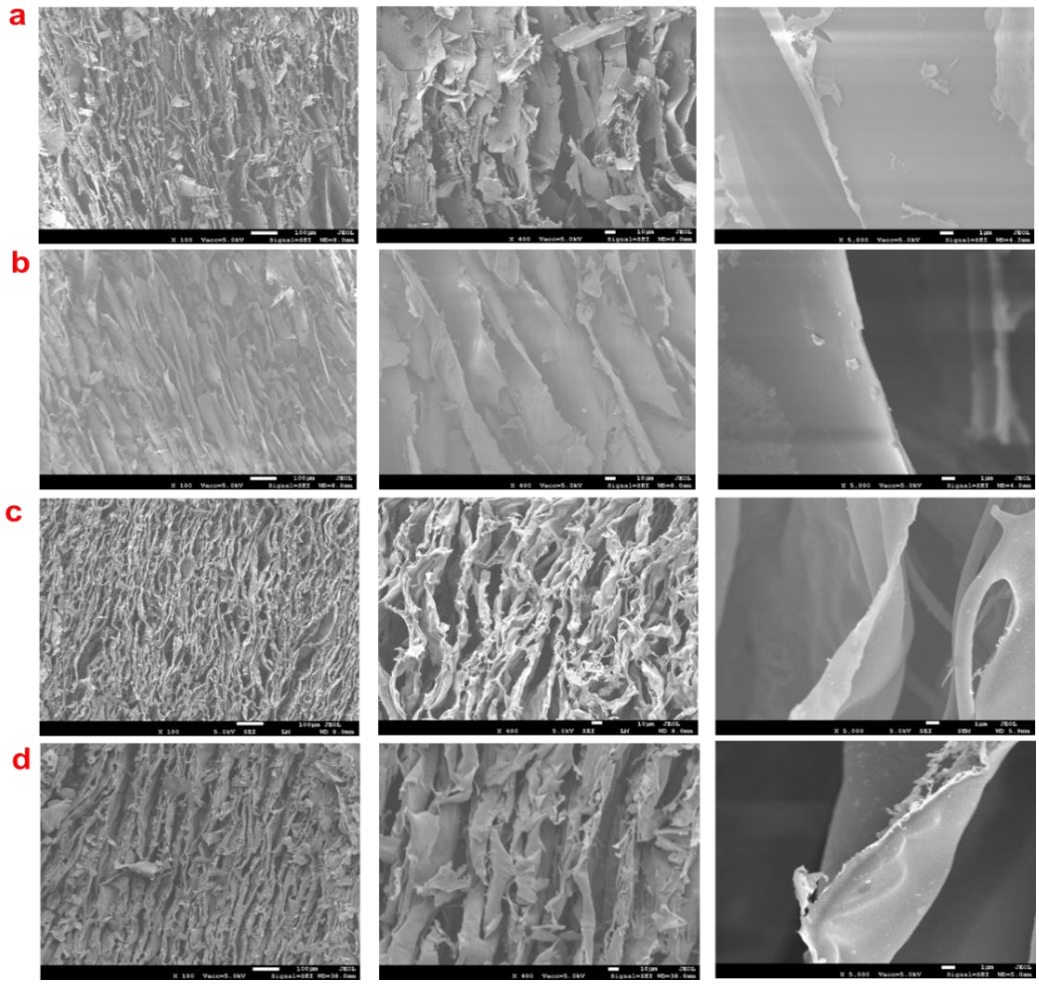

Fig. 2. SEM images in the longitudinal direction of the lignin foams derived from the aqueous suspensions of different lignin concentrations and the resultant LC foams: (a) lignin and (c) LC foams derived from the suspension with 18.5 mg/mL lignin; (b) lignin and (d) LC foams derived from the suspension with 37.0 mg/mL lignin. Scale bars in (a-d) are 100 μm, 10 μm and 1μm from left to the right column.

EMI SE characterizes the capability of attenuating electromagnetic waves of an EMI shielding material. The total EMI SE (SE_T) consists of shielding by reflection (SE_R) and shielding by absorption (SE_A), and influenced by multiple reflections, which are related to mobile charge carrier, electric (or magnetic) dipoles, and interfaces/surfaces in the shielding materials [13, 50]. Most waves underwent multiple reflections could eventually be absorbed by high-performance EMI shielding materials, and thus SE_T is usually the sum of SE_R and SE_A [10, 14]. Considering the

anistropic microsture, the X-band EMI SE of the honeycomb-like LC foams was first tested when all incident electromagnetic waves propagate along the transverse directions, i.e., normal to the pore alignment direction. As shown in Fig. 3a, EMI SE of the LC foams is independent of the frequency and increases with the lignin concentration. The SE_T values are 15.6 and 31.5 dB for the LC foams derived from 18.5 and 100.0 mg/mL lignin, respectively. EMI SE of the LC foams derived from 37.0 mg/mL lignin could also be higher than 20 dB, which corresponds to a 99 % attenuation of incident electromagnetic waves and is required for most commercial shielding applications. Obviously, higher lignin concentration can lead to thicker cell walls and hence more charge carriers interacting with the electromagnetic field for the LC foam, resulting in a higher SE_A and SE_R, which thus increases the EMI SE. Additionally, the micron-sized pores in the LC foams can also be beneficial to the multiple reflections of incident waves. This, combined with the considerable absorption ability of LC cell walls, can thus lead to a higher SE_A than SE_R, indicating an absorption-dominant shielding mechanism for the LC foams, which is similar to other types of carbon or conductive polymer composite foams [24, 31, 34].

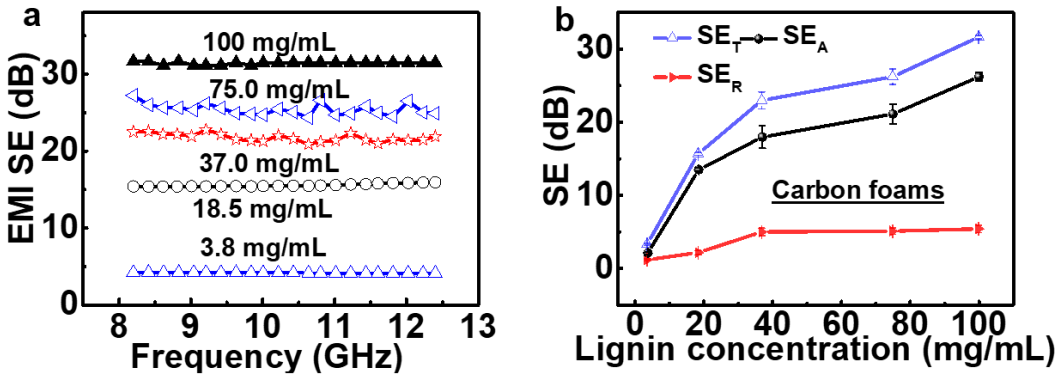

Fig. 3. (a) EMI SE of the LC foams derived from lignin suspensions with various concentrations; (b) EMI shielding performance (SE_T, SE_R, and SE_A) at the frequency of 10 GHz for the LC foams as a function of the lignin concentration in the suspensions.

3.2. Performance of Honeycomb-like RGO-doped LC Foams

3.2.1. Structure and Density

Compared with the LC foams that show a large volume shrinkage in carbonization, the RGO doping results in good dimensional and structural stabilities of the RGO-doped LC foams (Fig. 4a). As shown in Fig. 4b, the carbon foam density increases with the lignin concentration of the suspension used. By contrast, the density decreases with increasing the amount of RGO additives in the RGO-doped LC foams. The LC foam without doped RGO exhibits the largest volume shrinkage, which results in smaller volume or higher density than that of the RGO-doped LC foams. This shows that more RGO can lead to smaller volume shrinkage of the foams in carbonization, thereby keeping larger volume and lower density. Furthermore, the lightweight carbon-based foams can also be obtained in various shapes and sizes (Fig. 4c), which is suitable for a variety of applications that require shape adaptability.

Since GO can be well dispersed in the lignin-based cell walls of the lignin/GO foams, the corresponding RGO can be well dispersed and distributed in the composite cell walls for the LC/RGO foams. Compared with the smooth cell walls of the LC foams, wrinkle-like cell walls are observed for the RGO-doped LC foams, as shown in the SEM images in Figs. 4d, e. The RGO-doped LC foams also show relatively flat cell walls with more regular gaps in between than that in LC foams (Fig. 2c, d), which can be ascribed to the enhanced mechanical strength of graphene-doped cell walls. Similar microstructures can also be observed in the honeycomb-like RGO-doped LC foams with various LC/RGO contents (Fig. 4f, g). In short, RGO additives are considered to render the LC/RGO composite cell walls better mechanical strength, enhancing the dimensional and structural stability of the carbon foams. In addition, the distributed graphene layers have an excellent conductivity, providing a high potential to improve electrical and EMI shielding performance of the corresponding LC/RGO foams.

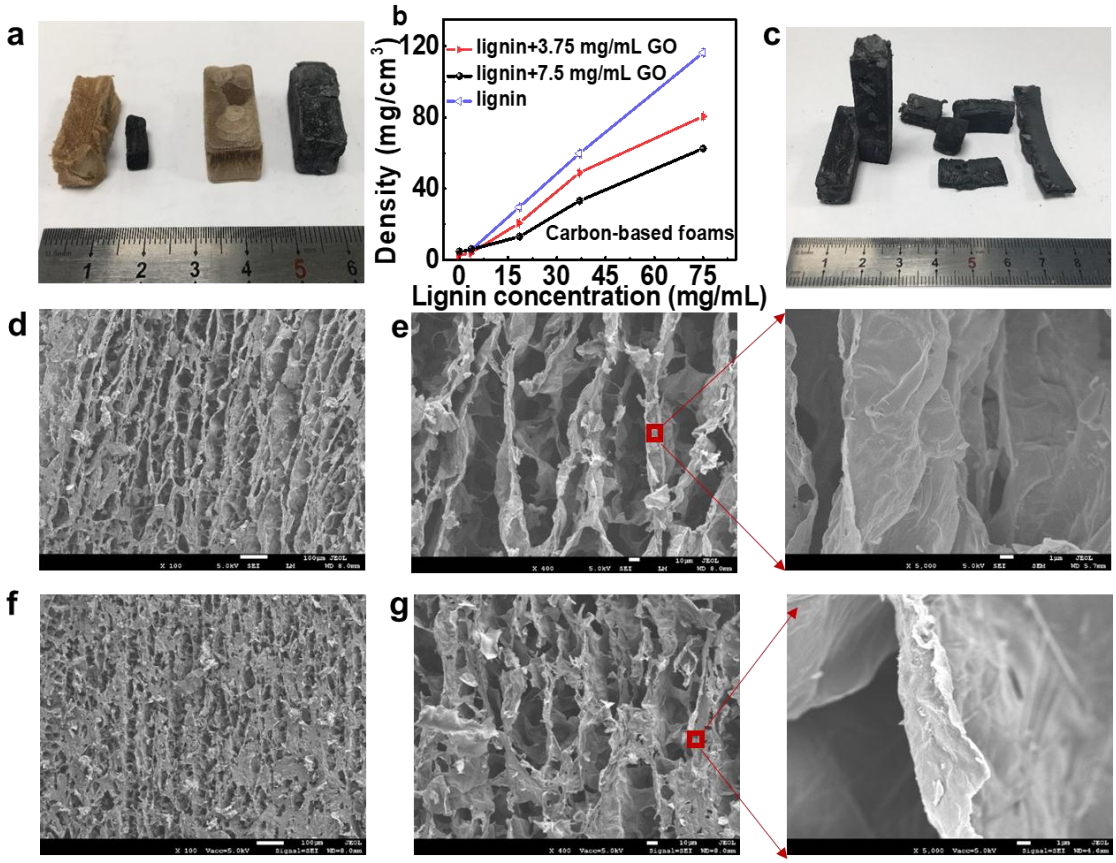

Fig. 4. Properties of the carbon foams: (a) image of the foams before and after thermal annealing (left to right: lignin, LC, GO-doped lignin and RGO-doped LC foams); (b) the densities of the carbon foams prepared from the suspensions with various concentrations of lignin and GO; (c) various shapes and sizes of the as-prepared LC/RGO foams. SEM images showing honeycomb-like microstructures of the LC/RGO foams prepared from suspensions with (d, e) 18.5 mg/mL lignin and 7.5 mg/mL GO, (f,g) 37.0 mg/mL lignin and 7.5 mg/mL GO. Scale bars in (d-g) are 100 µm, 10 µm and 1µm from left to the right column.

3.2.2 Electrical Conductivity

The influence of RGO doping on the electrical conductivity for the LC/RGO foams is shown in Fig. 5a. Excellent conductivity of the graphene layers can result in a significant increase of electrical conductivity of the foams. The conductivity of LC/RGO foams derived from the suspensions with 18.5 mg/mL lignin and various GO concentrations ranging from 3.75 to 11.25 mg/mL can reach 40.7 to 97.8 S/m,

more than one order of magnitude higher than that of the corresponding LC foams (~3.1 S/m). Such a significant increase in conductivity shows the vital roles of the graphene layers played in enhancing electrical properties, which would impact EMI shielding performance significantly. The increased lignin concentration can also result in significant improvement of the conductivity of LC/RGO foams (Fig. 5b). For instance, by fixing the GO concentration at 3.75 mg/mL and increasing lignin concentration from 3.7 to 75.0 mg/mL, the conductivity of the LC/RGO foams increases from 13.2 to 152.7 S/m. The LC/RGO foams derived from the suspension with 75.0 mg/mL lignin and 7.5 mg/mL GO can also achieve a very high conductivity of 391.3 S/m even at a low density of 62.5 mg/cm^3, which is much higher than the conductivity of the corresponding LC foam (~25.6 S/m), which is prepared at the same lignin concentration of 75.0 mg/mL and has the density of 116.0 mg/cm^3, and the corresponding RGO foams (~30.0 S/m), which is prepared at the same GO concentration of 7.5 mg/mL. In short, the wide-range adjustability of the lignin and GO concentrations in the starting materials can easily lead to a wide-range controllability of conductivity for the honeycomb-like carbon foams. The controllable high conductivities of the carbon foams show the great potential to achieve high-performance EMI shielding performance.

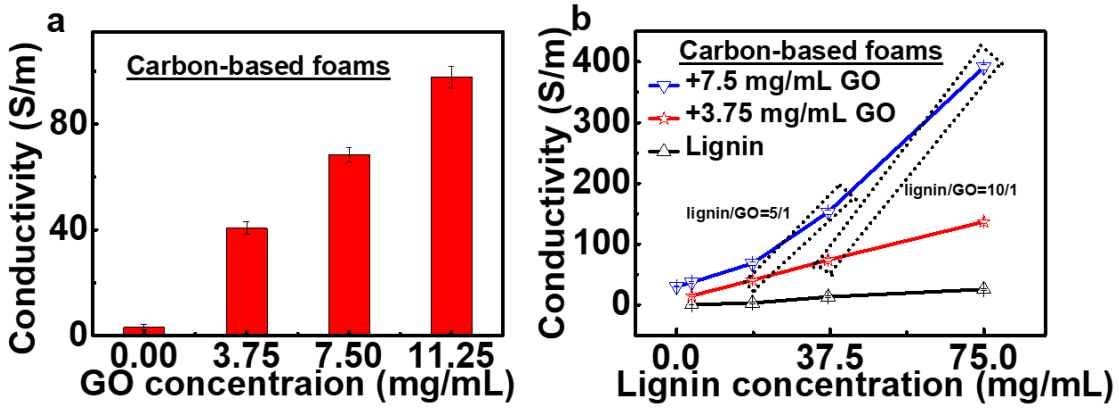

Fig. 5. Electrical conductivity of the carbon foams derived from the suspensions with various lignin and GO concentrations: (a) with lignin concentration of 18.5 mg/mL and various GO concentrations, (b) with various concentrations of lignin and GO (the lignin/GO mass ratios are 5 and 10, respectively, for the foams in the dotted boxes).

3.2.3. Mechanical performance

The alignment of cell walls and the starting lignin concentrations significantly affect mechanical properties of the honeycomb-like carbon foams. Longitudinal compressive moduli (compressed along the longitudinal direction) of the carbon foams are higher than the transverse ones (compressed normal to the longitudinal direction); typically, the former and the latter are around 427 and 130 kPa respectively for the LC/RGO foams obtained at 18.5 mg/mL lignin and 3.75 mg/mL GO concentrations (Fig. 6a). Since higher lignin concentrations can lead to more building blocks in the porous architectures, thereby much increasing the compressive modulus as shown in Fig. 6b. The apparent modulus of the carbon foams obtained at 7.5 mg/mL GO and various lignin concentrations from 18.5 to 75.0 mg/mL can reach 120 to 1470 kPa, compared with that of around 12 kPa for relevant RGO foams. However, higher LC content also enhance brittleness of the carbon foams because of the increased amount of amorphous carbon, which results in a lower yield strain.

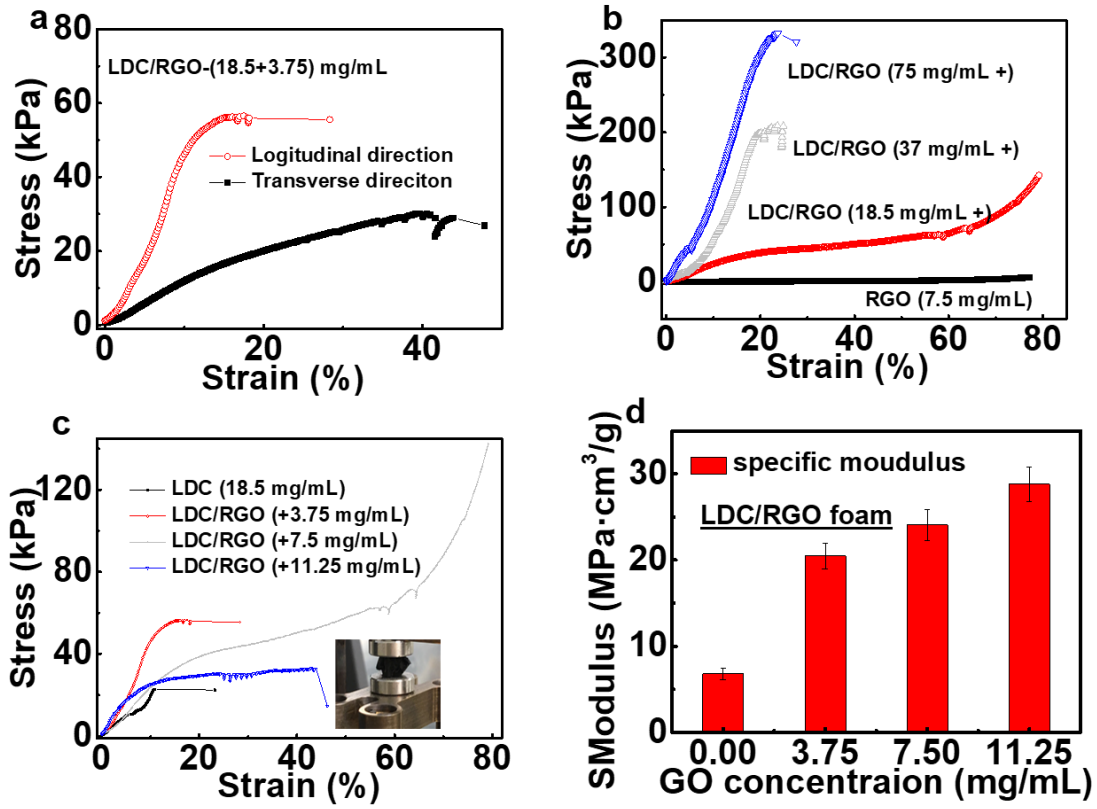

Fig. 6 Compression stress-strain curves of the honeycomb-like carbon foams obtained at various lignin and GO concentrations: (a) longitudinal and transverse compression curves at 18.5 mg/mL lignin and 3.75 mg/mL GO concentrations; longitudinal compression curves at (b) GO concentration of 7.5 mg/mL and various lignin concentrations and (c) lignin concentration of 18.5 mg/mL and various GO concentrations (the inset shows the collapsing of a LC foam under compression). (d)The apparent specific modulus (S-Modulus) of the carbon foams obtained at lignin concentration of 18.5 mg/mL and various GO concentrations.

To illustrate the effect of doped graphene on mechanical properties, longitudinal compression stress-strain curves of the honeycomb-like carbon foams obtained at 18.5 mg/mL lignin and various GO concentrations are shown in Fig. 6c. In contrast to the LC foams that collapse easily at low apparent compressive strain of around 10 %, the composite foams exhibit increased apparent yield strains. The carbon foams with a density of 13 mg/cm^3 obtained at 18.5 mg/mL lignin and 7.5 mg/mL GO concentrations are not damaged even at a high apparent strain of 80 %. The carbon

foams with density of 17 mg/cm^3 obtained at 18.5 mg/mL lignin and 11.25 mg/mL GO concentrations exhibit the highest apparent compressive modulus of 490 kPa, which is 245 % of that of the corresponding LC foams (~200 kPa) with a density of 29.2 mg/cm^3. The compressive performance of the foams is dependent on the graphene fraction and density of samples. To better gauge the influence of the RGO doping on the mechanical performance, apparent specific moduli of the foams, which refer to their apparent compressive moduli divided by the respective densities, respectively, are compared in Fig. 6d. Higher graphene contents lead to significantly enhanced apparent specific modulus.

3.2.4. EMI shielding performance and mechanism

Transverse EMI SE of the honeycomb-like carbon-based foams obtained at 18.5 mg/mL lignin and various GO concentrations is shown in Fig. 7a. It shows that the SE increases with graphene content. In comparison with an EMI SE of 15.6 dB for LC foams, SE values of the LC/RGO foams obtained at 3.75 and 11.25 mg/mL GO are as high as 36.4 and 60.4 dB, respectively. Since higher graphene content leads to significantly higher conductivity for the honeycomb-like foams, their SE_R and SE_A can be enhanced. In addition, conductivity mismatch between graphene and LC in the cell walls results in interfacial polarization loss at the interfaces [43, 56], benefiting the wave-absorption capability of foams. These characteristics will lead to higher SE_R, SE_A and SE_T of the carbon-based foams at a higher graphene content (Fig. 7b).

Considering anisotropic microstructure of the honeycomb-like carbon-based foams, EMI shielding performances in transverse (T-SE_T, T-SE_R, T-SE_A) and

longitudinal (L-SE_T, L-SE_R, L-SE_A) directions are also compared in Fig. 7b. The cell wall-void interfaces can promote multiple reflection of incident waves [13, 43], further increasing penetration loss of the waves for LC/RGO foams. Therefore, more multiple reflections occur when incident electromagnetic waves propagate along transverse direction, leading to enhanced T-SE_A. By contrast, SE_R values in different directions are similar due to their similar conductivities. Thus T-SE_T is higher than L-SE_T for the honeycomb-like carbon-based foams. Fig. 8a further shows that T-SE_T can be well controlled by adjusting their density/porosity, which is achieved easily by adjusting the water fraction of lignin/GO mixed suspensions. For the carbon foams derived from a fixed lignin/GO mass ratio of 10, the density of the free-standing foams can be as low as 14 mg/cm^3 while the EMI SE is higher than 20 dB. High SE with significantly decreased density leads to high SSE, which increases as density of the composite foams reduces, as shown in Fig. 8b. This demonstrates the important role played by the density/porosity in tuning EMI shielding performance.

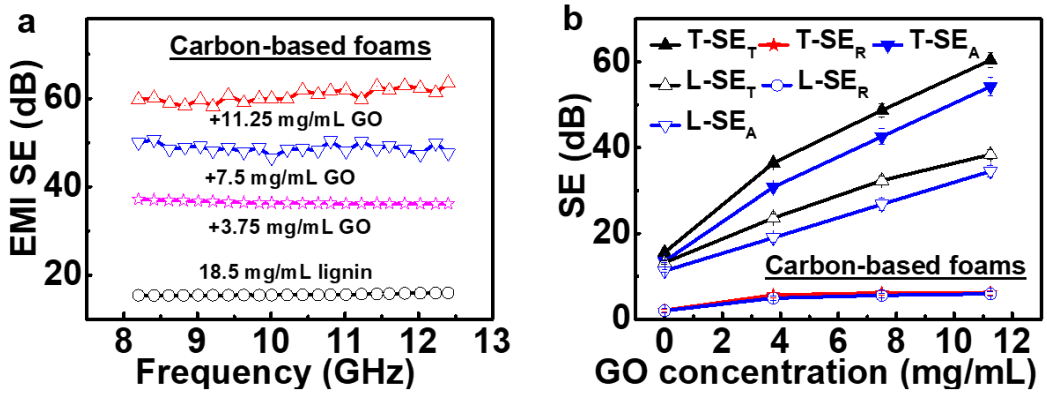

Fig. 7. EMI shielding performance of the honeycomb-like carbon-based foams: (a) transverse EMI SE in the X-band of the carbon-based foams obtained at 18.5 mg/mL lignin and various concentrations of GO, (b) and the SE_T, SE_A, and SE_R at the frequency of 10 GHz of these carbon-based foams in transverse and longitudinal directions.

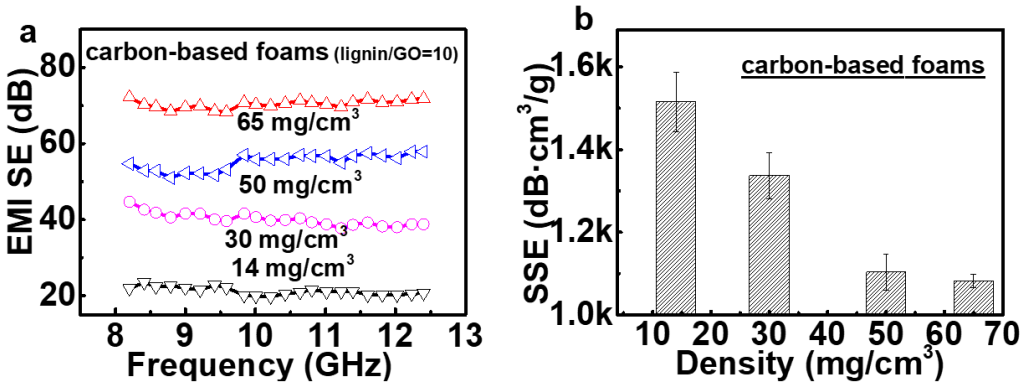

Fig. 8. Transverse EMI shielding performance of the LC/RGO foams at various densities when the initial mass ratio of the lignin to GO is 10: (a) EMI SE in the X-band and (b) SSE as a function of density.

Lignin concentration also significantly affects the EMI SE of the RGO-doped LC foams, as shown in Fig. 9a. EMI SE can reach 70.5 dB for the LC/RGO foams derived from 75.0 mg/mL lignin and 7.5 mg/mL GO, and at higher lignin concentrations, the SE values are higher than the upper detection limit of the instrument (80 dB). The widely varied EMI SE values of the carbon foams result in a very wide range of SSE values, as displayed in Fig. 9b. For example, SSE of the LC foams obtained at 18.5 mg/mL lignin and the LC/RGO foams obtained at 18.5 mg/mL lignin and 7.5 mg/mL GO are 532.9 and 3746.2 dB·cm^3/g, respectively, at the thickness of 2 mm. The highest SSE achieved for the LC/RGO foams is 5750 dB·cm^3/g, which far exceeds SSE values of other types of carbon foams ever reported, as shown in Fig. 9c and Table 1, and is also one of the top values among various types of shielding materials (Table S1).

Considering the thickness factor, SSE/*d* (SSE divided by the thickness) is calculated as a function of density and compared with that of other typical shielding

materials (Fig. 9d). Notably, the wide-range density controllability and easy adjustability of the composition of building blocks render the RGO-doped LC foams high SSE/*d* values ranging from 3634 to 28750 dB·cm^2/g with the corresponding EMI SE of > 30 dB. The highest SSE/*d* value for the RGO/LC foam is much higher than that of CNT sponge (4620 dB·cm^2/g) [36], graphene-based composite foams (5000 dB·cm^2/g) [14], copper and stainless steel sheet (32-28 dB·cm^2/g) [11], CuNi alloy foams (1160-1580 dB·cm^2/g) [57], and various fillers embedded polymer composites [58]. The super high SSE/*d* value of our honeycomb-like carbon-based foams (Table 1, Table S1) can be ascribed to the high-efficiency utilization of cell wall-void interfaces, substantial interfaces between LC and doped graphene, and significantly enhanced conductivity of LC/RGO foams. Combined with the excellent mechanical performance and structural controllability, as well as the low-cost and renewable nature of lignin, the RGO/LC foams show great potential for lightweight, robust, and high-performance EMI shielding applications.

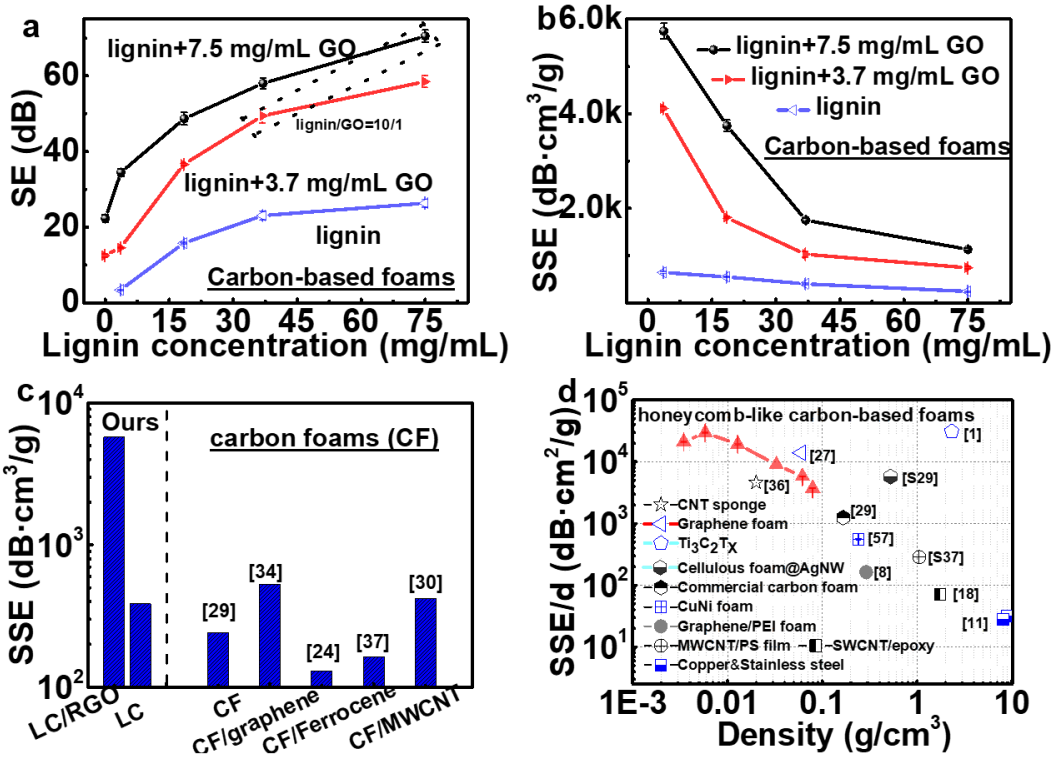

Fig. 9. Transverse EMI shielding performance of the honeycomb-like carbon-based foams: (a) transverse EMI SE in the X-band (the mass ratio of the lignin and GO is 10 for the carbon-based foams in the dotted box) and (b) relevant SSE at the frequency of 10 GHz of the carbon foams derived from various concentrations of lignin and GO; (c) SSE of our LC-based carbon foams and other reported typical carbon foams (CF); (d) SSE/*d* values as a function of density for the typical shielding materials and our LC-based foams.

Table 1. EMI shielding performance of our LC-based carbon foams in comparison with that of typical carbon-based porous architectures

Materials	SE (dB)	Thickness (mm)	SSE ($dB \cdot cm^3/g$)	Surface SSE ($dB \cdot cm^2/g$)	Ref.
Commercial carbon foam	40	2	241	1205	[29]
Phthalonitrile-based carbon foam	51.2	2	341	1707	[34]
Sugarcane-derived Carbon foam	51	10	455	455	[39]
Carbon texture/graphene aerogel	37	3.0	529	1762	[24]
Carbon/graphene foams	51	0.073	84	11452	[31]
	24	0.024	39	16393	
Carbon/ferrocene foam	81	2.75	130	473	[37]
MWCNT-decorated carbon foam	85	2.75	164	594	[30]
Wood-derived carbon foam (WDC)	~53	5	~408	815	[33]
WDC coated with graphene and AgNW	~60	5	465	930	[33]
Graphene foam	25.2	0.3	420.0	14000	[27]
Sponged-supported RGO aerogel	24	12	1437	1198	[59]
CNF mat	81.1	4.6	370	804	[35]
	52.2	2.9	390	1361	
CNT sponge	22	2.38	1100	4622	[36]
Honeycomb-like lignin-based carbon/graphene foams	**34.5**	**2**	**5750**	**28750**	**This work**
	48.7	**2**	**3746**	**18731**	
	70.5	**2**	**1128**	**5642**	
	60.4	**2**	**3555**	**17774**	

4. Conclusions

Lightweight and robust honeycomb-like RGO-doped LC foams could be readily prepared via the ice-templating, freeze-drying and carbonization. The dimensions, composition, and density of the foams could be easily adjusted. By manipulating the density, high electrical conductivity and good mechanical properties could be achieved at relatively high LC/RGO mass ratio. The RGO layers dispersed in the LC-based cell walls give rise to significantly enhanced electrical conductivity of the

carbon foams, benefiting the EMI shielding performance. Interfaces between the LC and RGO also induce enhanced interfacial polarization loss to incident electromagnetic waves. The aligned pores and cell walls in the honeycomb-like foams promote multiple reflections of the incident electromagnetic waves in the porous architectures, further facilitating wave-absorption ability. As a result, excellent EMI shielding performance is achieved for the LC-based foams. X-band EMI SE of the 2 mm thick LC-based foams can reach 28.5 to 70.5 dB at low densities, and the highest SSE/*d* can reach up to 28750 dB·cm^2/g, far higher than those of other types of carbon foams and most shielding materials ever reported. The excellent EMI shielding performance of the LC-based foams, combined with their good mechanical strength, ease of fabrication and facile structural tunability demonstrate that low-cost, sustainable biomass-derived lightweight carbon foams have high potential for a broad range of EMI shielding applications.

ACKNOWLEDGMENTS

This work was supported by Science and Engineering Research Council of the Agency for Science, Technology and Research (A*STAR) Singapore under Public Sector Research Funding (PSF) Grant No. 1521200077. S. I. S. Shahabadi thanks A*Star for providing Ph.D. scholarships in the course of this work.

REFERENCES

[1] F. Shahzad, M. Alhabeb, C.B. Hatter, B. Anasori, S. Man Hong, C.M. Koo, et al., Electromagnetic interference shielding with 2D transition metal carbides (MXenes), Science 353(6304) (2016) 1137-1140.

[2] J. Liu, H.B. Zhang, R. Sun, Y. Liu, Z. Liu, A. Zhou, et al., Hydrophobic, Flexible, and Lightweight MXene Foams for High-Performance Electromagnetic-Interference Shielding, Adv. Mater. 29(38) (2017) 1702367.

[3] R. Sun, H.-B. Zhang, J. Liu, X. Xie, R. Yang, Y. Li, et al., Highly Conductive Transition Metal Carbide/Carbonitride(MXene)@polystyrene Nanocomposites Fabricated by Electrostatic Assembly for Highly Efficient Electromagnetic Interference Shielding, Adv. Funct. Mater. 27(45) (2017) 1702807.

[4] Q. Song, F. Ye, X. Yin, W. Li, H. Li, Y. Liu, et al., Carbon Nanotube-Multilayered Graphene Edge Plane Core-Shell Hybrid Foams for Ultrahigh-Performance Electromagnetic-Interference Shielding, Adv. Mater. (2017) 1701583.

[5] Y. Yang, M.C. Gupta, K.L. Dudley, R.W. Lawrence, Novel Carbon Nanotube−Polystyrene Foam Composites for Electromagnetic Interference Shielding, Nano Lett. 5(11) (2005) 2131-2134.

[6] Y. Yang, M.C. Gupta, K.L. Dudley, R.W. Lawrence, Conductive Carbon Nanofiber–Polymer Foam Structures, Adv. Mater. 17(16) (2005) 1999-2003.

[7] A. Ameli, M. Nofar, S. Wang, C.B. Park, Lightweight polypropylene/stainless-steel fiber composite foams with low percolation for efficient electromagnetic interference shielding, ACS Appl. Mater. Interfaces 6(14) (2014) 11091-100.

[8] J. Ling, W. Zhai, W. Feng, B. Shen, J. Zhang, W. Zheng, Facile preparation of lightweight microcellular polyetherimide/graphene composite foams for electromagnetic interference shielding, ACS Appl. Mater. Interfaces 5(7) (2013) 2677-84.

[9] B. Shen, W. Zhai, M. Tao, J. Ling, W. Zheng, Lightweight, multifunctional polyetherimide/graphene@Fe3O4 composite foams for shielding of electromagnetic pollution, ACS Appl. Mater. Interfaces 5(21) (2013) 11383-91.

[10] H.B. Zhang, Q. Yan, W.G. Zheng, Z. He, Z.Z. Yu, Tough graphene-polymer microcellular foams for electromagnetic interference shielding, ACS Appl. Mater. Interfaces 3(3) (2011) 918-24.

[11] X. Shui, D.D.L. Chung, Nickel filament polymer-matrix composites with low surface impedance and high electromagnetic interference shielding effectiveness, J. Electr. Mater. 26(8) (1997) 928-934.

[12] J.-M. Thomassin, C. Jérôme, T. Pardoen, C. Bailly, I. Huynen, C. Detrembleur, Polymer/carbon based composites as electromagnetic interference (EMI) shielding materials, Mater. Sci. Eng. R. 74(7) (2013) 211-232.

[13] Z. Zeng, H. Jin, M. Chen, W. Li, L. Zhou, Z. Zhang, Lightweight and Anisotropic Porous MWCNT/WPU Composites for Ultrahigh Performance Electromagnetic Interference Shielding, Adv. Funct. Mater. 26(2) (2016) 303-310.

[14] Z. Chen, C. Xu, C. Ma, W. Ren, H.M. Cheng, Lightweight and flexible graphene foam composites for high-performance electromagnetic interference shielding, Adv. Mater. 25(9) (2013) 1296-300.

[15] Z. Zeng, H. Jin, M. Chen, W. Li, L. Zhou, X. Xue, et al., Microstructure Design of Lightweight, Flexible, and High Electromagnetic Shielding Porous Multiwalled Carbon Nanotube/Polymer Composites, Small 13(34) (2017) 1701388.

[16] D.-X. Yan, H. Pang, B. Li, R. Vajtai, L. Xu, P.-G. Ren, et al., Structured Reduced Graphene Oxide/Polymer Composites for Ultra-Efficient Electromagnetic Interference Shielding, Adv. Funct. Mater. 25(4) (2015) 559-566.

[17] S.-T. Hsiao, C.-C.M. Ma, H.-W. Tien, W.-H. Liao, Y.-S. Wang, S.-M. Li, et al., Using a non-covalent modification to prepare a high electromagnetic interference shielding performance graphene nanosheet/water-borne polyurethane composite, Carbon 60 (2013) 57-66.

[18] Y. Huang, N. Li, Y. Ma, F. Du, F. Li, X. He, et al., The influence of single-walled carbon nanotube structure on the electromagnetic interference shielding efficiency of its epoxy composites, Carbon 45(8) (2007) 1614-1621.

[19] N. Li, Y. Huang, F. Du, X. He, X. Lin, H. Gao, et al., Electromagnetic Interference (EMI) Shielding of Single-Walled Carbon Nanotube Epoxy Composites, Nano Lett. 6(6) (2006) 1141-1145.

[20] J.G. Park, J. Louis, Q. Cheng, J. Bao, J. Smithyman, R. Liang, et al., Electromagnetic interference shielding properties of carbon nanotube buckypaper composites, Nanotechnology 20(41) (2009) 415702.

[21] Y. Chen, H.-B. Zhang, Y. Yang, M. Wang, A. Cao, Z.-Z. Yu, High-Performance Epoxy Nanocomposites Reinforced with Three-Dimensional Carbon Nanotube Sponge for Electromagnetic Interference Shielding, Adv. Funct. Mater. 26(3) (2016) 447-455.

[22] D.-X. Yan, P.-G. Ren, H. Pang, Q. Fu, M.-B. Yang, Z.-M. Li, Efficient electromagnetic interference shielding of lightweight graphene/polystyrene composite, J. Mater. Chem. 22(36) (2012) 18772.

[23] W.-L. Song, M.-S. Cao, M.-M. Lu, S. Bi, C.-Y. Wang, J. Liu, et al., Flexible graphene/polymer composite films in sandwich structures for effective electromagnetic interference shielding, Carbon 66 (2014) 67-76.

[24] W.-L. Song, X.-T. Guan, L.-Z. Fan, W.-Q. Cao, C.-Y. Wang, M.-S. Cao, Tuning three-dimensional textures with graphene aerogels for ultra-light flexible graphene/texture composites of effective electromagnetic shielding, Carbon 93 (2015) 151-160.

[25] Y.-J. Wan, P.-L. Zhu, S.-H. Yu, R. Sun, C.-P. Wong, W.-H. Liao, Ultralight, super-elastic and volume-preserving cellulose fiber/graphene aerogel for high-performance electromagnetic interference shielding, Carbon 115 (2017) 629-639.

[26] H. Chen, Z. Huang, Y. Huang, Y. Zhang, Z. Ge, B. Qin, et al., Synergistically assembled MWCNT/graphene foam with highly efficient microwave absorption in both C and X bands, Carbon 124 (2017) 506-514.

[27] B. Shen, Y. Li, D. Yi, W. Zhai, X. Wei, W. Zheng, Microcellular graphene foam for improved broadband electromagnetic interference shielding, Carbon 102 (2016) 154-160.

[28] Y. Zhang, Y. Huang, T. Zhang, H. Chang, P. Xiao, H. Chen, et al., Broadband and tunable high-performance microwave absorption of an ultralight and highly compressible graphene foam, Adv. Mater. 27(12) (2015) 2049-53.

[29] F. Moglie, D. Micheli, S. Laurenzi, M. Marchetti, V. Mariani Primiani, Electromagnetic shielding performance of carbon foams, Carbon 50(5) (2012) 1972-1980.

[30] R. Kumar, S.R. Dhakate, T. Gupta, P. Saini, B.P. Singh, R.B. Mathur, Effective improvement of the properties of light weight carbon foam by decoration with multi-wall carbon nanotubes, J. Mater. Chem. A 1(18) (2013) 5727.

[31] Y. Li, B. Shen, X. Pei, Y. Zhang, D. Yi, W. Zhai, et al., Ultrathin carbon foams for effective electromagnetic interference shielding, Carbon 100 (2016) 375-385.

[32] Q. Li, L. Chen, J. Ding, J. Zhang, X. Li, K. Zheng, et al., Open-cell phenolic carbon foam and electromagnetic interference shielding properties, Carbon 104 (2016) 90-105.

[33] Y. Yuan, X. Sun, M. Yang, F. Xu, Z. Lin, X. Zhao, et al., Stiff, Thermally Stable and Highly Anisotropic Wood-Derived Carbon Composite Monoliths for

Electromagnetic Interference Shielding, ACS Appl. Mater. Interfaces 9(25) (2017) 21371-21381.

[34] L. Zhang, M. Liu, S. Roy, E.K. Chu, K.Y. See, X. Hu, Phthalonitrile-Based Carbon Foam with High Specific Mechanical Strength and Superior Electromagnetic Interference Shielding Performance, ACS Appl. Mater. Interfaces 8(11) (2016) 7422-30.

[35] X. Hong, D.D.L. Chung, Carbon nanofiber mats for electromagnetic interference shielding, Carbon 111 (2017) 529-537.

[36] M. Crespo, M. González, A.L. Elías, L. Pulickal Rajukumar, J. Baselga, M. Terrones, J. Pozuelo, Ultra-light carbon nanotube sponge as an efficient electromagnetic shielding material in the GHz range, Phys. Stat. Sol. (RRL) 8(8) (2014) 698-704.

[37] R. Kumar, S.R. Dhakate, P. Saini, R.B. Mathur, Improved electromagnetic interference shielding effectiveness of light weight carbon foam by ferrocene accumulation, RSC Adv. 3(13) (2013) 4145.

[38] A. Ameli, P.U. Jung, C.B. Park, Electrical properties and electromagnetic interference shielding effectiveness of polypropylene/carbon fiber composite foams, Carbon 60 (2013) 379-391.

[39] Y.-Q. Li, Y.A. Samad, K. Polychronopoulou, K. Liao, Lightweight and Highly Conductive Aerogel-like Carbon from Sugarcane with Superior Mechanical and EMI Shielding Properties, ACS Sust. Chem. Eng. 3(7) (2015) 1419-1427.

[40] W. Liu, R. Zhou, D. Zhou, G. Ding, J.M. Soah, C.Y. Yue, et al., Lignin-assisted direct exfoliation of graphite to graphene in aqueous media and its application in polymer composites, Carbon 83 (2015) 188-197.

[41] F. Shahzad, P. Kumar, Y.H. Kim, S.M. Hong, C.M. Koo, Biomass-Derived Thermally Annealed Interconnected Sulfur-Doped Graphene as a Shield against Electromagnetic Interference, ACS Appl. Mater. Interfaces 8(14) (2016) 9361-9.

[42] S.X. Wang, L. Yang, L.P. Stubbs, X. Li, C. He, Lignin-Derived Fused Electrospun Carbon Fibrous Mats as High Performance Anode Materials for Lithium Ion Batteries, ACS Appl. Mater. Interfaces 5(23) (2013) 12275–12282.

[43] Z. Zeng, C. Wang, Y. Zhang, P. Wang, S.I.S. Shahabadi, Y. Pei, et al., Ultralight and Highly Elastic Graphene/Lignin-Derived Carbon Nanocomposite Aerogels with Ultrahigh Electromagnetic Interference Shielding Performance, ACS Appl. Mater. Interfaces 10(9) (2018) 8205-8213.

[44] S. Deville, E. Saiz, R.K. Nalla, A.P. Tomsia, Freezing as a Path to Build Complex Composites, Science 311(5760) (2006) 515-518.

[45] H. Zhang, A.I. Cooper, Aligned Porous Structures by Directional Freezing, Adv. Mater. 19(11) (2007) 1529-1533.

[46] H. Zhang, I. Hussain, M. Brust, M.F. Butler, S.P. Rannard, A.I. Cooper, Aligned two- and three-dimensional structures by directional freezing of polymers and nanoparticles, Nat. Mater. 4(10) (2005) 787-93.

[47] Z. Zeng, S.I. Seyed Shahabadi, B. Che, Y. Zhang, C. Zhao, X. Lu, Highly Stretchable, Sensitive Strain Sensors with Wide Linear Sensing Region Based on

Compressed Anisotropic Graphene Foam/Polymer Nanocomposites, Nanoscale 9(2017) 17396-17404.

[48] L. Qiu, J.Z. Liu, S.L. Chang, Y. Wu, D. Li, Biomimetic superelastic graphene-based cellular monoliths, Nat. Commun. 2012, 3, 1241.

[49] J. Kuang, L. Liu, Y. Gao, D. Zhou, Z. Chen, B. Han, et al., A hierarchically structured graphene foam and its potential as a large-scale strain-gauge sensor, Nanoscale 5 (2013) 12171-7.

[50] Z. Zeng, M. Chen, H. Jin, W. Li, X. Xue, L. Zhou, et al., Thin and Flexible Multi-walled Carbon Nanotube/Waterborne Polyurethane Composites with High-performance Electromagnetic Interference Shielding, Carbon 2016, 96, 768-777.

[51] H. Li, D. Yuan, C. Tang, S. Wang, J. Sun, Z. Li, et al., Lignin-derived Interconnected Hierarchical Porous Carbon Monolith with Large Areal/Volumetric Capacitances for Supercapacitor, Carbon 2016, 100, 151-157.

[52] J. Sun, C. Wang, L.P. Stubbs, C. He, Carboxylated Lignin as an Effective Cohardener for Enhancing Strength and Toughness of Epoxy, Macromol. Mater. Eng. 2017, 302, 1700341.

[53] D.K. Shen, S. Gu, K.H. Luo, S.R. Wang, M.X. Fang, The pyrolytic degradation of wood-derived lignin from pulping process, Bioresource Technol. 2010, 101, 6136-46.

[54] J. Cao, G. Xiao, X. Xu, D. Shen, B. Jin, Study on carbonization of lignin by TG-FTIR and high-temperature carbonization reactor, Fuel Process. Technol. 2013, 106, 41-47.

[55] H. Li, J. Sun, C. Wang, S. Liu, D. Yuan, X. Zhou, et al., High Modulus, Strength, and Toughness Polyurethane Elastomer Based on Unmodified Lignin, ACS Sustain. Chem. Eng. 2017, 5, 7942−7949.

[56] N. Yousefi, X. Sun, X. Lin, X. Shen, J. Jia, B. Zhang, et al., Highly aligned graphene/polymer nanocomposites with excellent dielectric properties for high-performance electromagnetic interference shielding, Adv. Mater. 26(31) (2014) 5480-7.

[57] K. Ji, H. Zhao, J. Zhang, J. Chen, Z. Dai, Fabrication and electromagnetic interference shielding performance of open-cell foam of a Cu–Ni alloy integrated with CNTs, Appl. Surf. Sci. 311 (2014) 351-356.

[58] Z. Zeng, M. Chen, Y. Pei, S.I. Seyed Shahabadi, B. Che, P. Wang, et al., Ultralight and Flexible Polyurethane/Silver Nanowire Nanocomposites with Unidirectional Pores for Highly Effective Electromagnetic Shielding, ACS Appl. Mater. Interfaces 9(37) (2017) 32211-32219.

[59] C. Liu, S. Ye, J. Feng, The Preparation of Compressible and Fire-Resistant Sponge-Supported Reduced Graphene Oxide Aerogel for Electromagnetic Interference Shielding, Chem. Asian. J. 11(18) (2016) 2586-93.